

See discussions, stats, and author profiles for this publication at: <https://www.researchgate.net/publication/234545815>

Determination of the pattern speed in the grand design spiral galaxy NGC 4321.

Article in *Astronomy and Astrophysics* · March 1995

CITATIONS

7

READS

63

4 authors, including:



S. García-Burillo

OAN-IGN

478 PUBLICATIONS 17,997 CITATIONS

[SEE PROFILE](#)



Francoise Combes

Observatoire de Paris

1,230 PUBLICATIONS 33,087 CITATIONS

[SEE PROFILE](#)

Determination of the pattern speed in the grand design spiral galaxy NGC 4321

M.J. Sempere^{1,2}, S. García-Burillo³, F. Combes¹, and J.H. Knapen²

¹ Observatoire de Meudon, F-92195 Meudon Principal Cedex, France

² IAC, Instituto de Astrofísica de Canarias, E-38200 La Laguna, Tenerife, Spain

³ Centro Astronómico de Yebes. IGN, E-19080 Guadalajara, Spain

Received 23 March 1994 / Accepted 5 September 1994

Abstract. Measurement of pattern speeds has been an observational imperative in the last years since a clear determination of the corotation resonance radius will give some insight in the nature of density waves and in the mechanism of their maintenance.

In this paper we analyse in detail the practical application to the grand design spiral NGC 4321 of two different methods, intended to derive the pattern speed (Ω_p) of its wave-based structure.

The first method, based on the change of sign of the radial streaming motions beyond the corotation circle, is an observational diagnostic discussed by Canzian (1993). The final morphology of the residual velocity field after subtraction of the rotation curve from the observed HI velocity field is analyzed in order to find the signature of two different morphological regions delimited by the corotation, as predicted by the theory.

The first successful application of this test to a real galaxy is presented. We have estimated a value for $\Omega_p \sim 20 \text{ km s}^{-1} \text{ kpc}^{-1}$ that locates corotation in the middle of the disc ($R_{CR} = 8 - 11 \text{ kpc}$). The only restriction for a more accurate determination comes from the intrinsic nature of the galaxy. The central bar potential distorts the spiral arm structure and the corotation is not a narrow, but a relatively extended region.

The second method, involving numerical simulations of the molecular cloud hydrodynamics, and supplying the behaviour of the neutral gas in the central parts of the galaxy, complete the observational information. This technique consists of a model fitting of the spiral gas response, the free parameter being Ω_p . The best fit solution is also obtained for $\Omega_p \sim 20 \text{ km s}^{-1} \text{ kpc}^{-1}$.

From this estimate we definitely validate the picture where the stellar bar ends within the corotation and the outer spiral structure, stretching out from the bar, lies outside the corotation circle.

The reassuring agreement in the solutions obtained using the two methods allows us to be optimistic about the applicability of the Canzian test as a method to detect the presence of density

waves in the discs of “real” galaxies and to derive their pattern speeds with reasonable accuracy.

Key words: galaxies: kinematics and dynamics – galaxies: spiral – galaxies: individual, NGC 4321 – galaxies: ISM – radio lines: galaxies

1. Introduction

Although density wave theory (DWT) has become the proper theoretical scenario to explain many of the observational features of the grand design spiral galaxies (spiral arms, dust inter-arm spurs, bars, streaming motions, etc...), a conclusive determination of the pattern speed of a spiral wave (Ω_p , a key parameter defining the wave-based spiral structure) has not been obtained so far in any galaxy.

There exist different observational methods to derive the value of Ω_p in a spiral galaxy disc, but whenever these tests have been applied to a particular object, they have given different, if not clearly contradictory, results.

We can shortly mention a few illustrative examples. In the case of the grand design galaxy M 81, summarized by Canzian (1993), several authors used different methods based on photometric or kinematic observational data, only to find values of R_{CR} varying from 7.2 to 11.3 kpc, without reaching a consensus. Kent (1987) and Kent & Glaudell (1989), tried to determine the pattern speed of the SO galaxy NGC 936. Employing the method proposed by Tremaine & Weinberg (1985), based on the stellar kinematics of the bar, a value of $\Omega_p=140 \text{ km s}^{-1} \text{ kpc}^{-1}$ was obtained. A second method based on a dynamical model of the galaxy, restricted values of the pattern speed to $\Omega_p=38-64 \text{ km s}^{-1} \text{ kpc}^{-1}$, with the latter value preferred (and Ω_p dependent on the mass-to-light ratio adopted). Elmegreen et al. (1989) proposed another method that consists in identifying symmetrical regions of enhanced star formation with resonances. A modified version of this method, has been used in NGC 628 and NGC

Send offprint requests to: M.J. Sempere

3992 by Cepa & Beckman (1990) and in M 51 by Knapen et al. (1992). They showed that the strongly peaked profiles that result from plotting the arm-interarm ratio of massive star formation could be identified with density wave resonances. However, this technique depends heavily on the symmetry in the star forming region pattern along the main spiral arms.

As a conclusion, we can say that there seem to be clear observational conflicts to derive values of pattern speeds (Canzian 1993).

In a previous paper (García-Burillo et al. (1993), hereafter called Paper I) we discussed the validity of three different methods used to identify and locate the position of the main resonances in the discs of grand design spiral galaxies, applied to one particular object: NGC 4321.

We assumed that there exists a well defined wave mode in this galaxy, and not only sheared spiral waves. This is justified since the galaxy is barred. However we cannot discard the co-existence of various wave modes, with different pattern speeds in this galaxy. Friedli & Martinet (1993) and Combes (1994), have studied the possible dynamical origin if bars within bars in lenticular and spiral galaxies and interpreted their existence as a signature of the secular evolution of gaseous and stellar discs. In this scenario the inner stellar bar detected by Pierce (1986), might be rotating faster than the main bar and the spiral structure of the disc. This does not prevent a fit of the slower main mode, however. It is also possible that the outer parts are perturbed by tidal interactions. At least 6 dwarf galaxies within a distance of 5 galactic radii from the centre of NGC 4321 can be seen in optical pictures. Nevertheless, it has not been proved so far if any of these galaxies are potentially interacting with NGC 4321 nor whether they could consequently excite secondary wave modes in the main galaxy disc.

The first method relies on the optical identification of the wave resonances in the disc, in particular, the identification of spurs that might be related to the orbit crowding in the vicinity of the 4:1 resonances, i.e., the radius at which $\Omega = \Omega_p - \kappa/4$ (see Elmegreen et al. 1989). These spurs have been identified by Elmegreen and collaborators in the enhanced optical pictures of NGC 4321 and helped them to derive the value of Ω_p .

The second method, extensively analyzed in Paper I, is based on the detection of the sign reversal of the radial streaming motions induced in the gas flow by the spiral pattern. This should occur when we go beyond the corotation circle (on the contrary, the tangential component of the streaming velocities experiences no change of sign). We made a full sampled map using the $2 \rightarrow 1$ and $1 \rightarrow 0$ transitions of CO of a region covering the presumed kinematical minor axis of the galaxy NGC 4321. By definition, along the minor axis only the radial components of the velocities in the plane of the gas disc have a non-zero projection along the line of sight: therefore, the detection of the sign reversal predicted by the density wave theory should then be possible. A modified "two-dimensional" version of this observational test has been discussed by Canzian (1993). After subtracting the axisymmetric velocity field solely due to the circular rotation of the gas, now we have access to the residual velocity pattern obtained in the whole galaxy disc (not only the

minor axis region). Based on the same effect of sign reversal of streaming motions limited to the radial in-plane component, we expect to have one approaching-receding spiral arm pair inside corotation, and outside corotation an ensemble of three approaching-receding spiral arm pairs (see below).

In Paper I, we also advanced the preliminary results of the application of a third independent method to derive the value of pattern velocities in spiral galaxy discs. This original method involves numerical simulations of the evolution of the molecular gas disc under the action of the spiral potential taken as close as possible to the real potential. The degree of agreement between the simulated gas disc and the gas response seen in the observations allowed us to fix, in parameter space of the fit, a value for Ω_p .

The values obtained for the corotation radius (R_{CR} , measured in the plane of the galaxy) with the three methods were hardly compatible. From the simulations fit we derived a value for R_{CR} similar to the one inferred from the identification of resonances features in the optical picture by Elmegreen and collaborators ($R_{CR} \simeq 120''$). The apparent absence of the corotation signature in the CO position-velocity diagram along the minor axis, led us to conclude that the corotation was at the outer disc ($R_{CR} \geq 160''$). We advance the following arguments to resolve this paradox:

- 1) An analysis of the particle-orbits plot obtained for the best fit solution from simulations of the gas disc, showed that what can be called the "corotation region" has a quite large radial extent. The interval (in galactic radii) where there should be a transition between oval-like orbits (typical of regions inside corotation) and "figure-eight" orbits (corresponding to regions outside corotation) is so exceptionally large, that only the observations of the outer disc gas might show the expected reversal of the radial streaming motions. Unfortunately the radial extent of the CO source is limited, and little CO can be detected at the outer disc. We must use imperatively a tracer of the neutral gas abundant enough to be detected at the outer disc, such HI.
- 2) The two-arm spiral structure appears severely distorted by the central bar potential. The observed CO kinematics gives a hint on the strength of the bar distortion: strong non-circular motions suggesting the presence of elliptical orbits are detected within the inner $R \simeq 60''$. The numerical simulations show again that the cloud orbits (in the rotating frame) tend to be aligned with the bar axis. The pitch angle of both gaseous spiral arms changes significantly with the azimuth. We strongly emphasize that, so far, the reversal of radial streaming motions has only been shown to occur and be "detectable" for model galaxies having smooth spiral arms with a constant pitch angle (see Canzian 1993).

From points 1) and 2), we concluded that the apparent absence of a sign change in the radial streaming motions visible in the CO position-velocity diagram, cannot be interpreted as a proof of the corotation lying at the outer disc ($R_{CR} \geq 160''$).

In the present paper we analyse the kinematics of HI in the disc of NGC 4321. We will study and apply the Canzian test

to the NGC 4321 HI data cube, which would provide a clear determination of the position of corotation, in the case of a wave-based structure.

We discuss the results of 3-D numerical simulations of the molecular gas dynamics using three cloud-cloud collision algorithms. As we now have complete two-dimensional information on the observed response of the HI gas to the spiral wave, the results of the fitting procedure employed to derive a value of Ω_p , are more reliable. We will also study the complex H α distribution (especially at the nucleus) and its relation with galaxy dynamics.

Another part of this paper is devoted to study the molecular cloud dynamics in the “simulated” galaxy, more specifically we will study the departures from circular motions and the variation of velocity dispersion in the galaxy disc (its origin and possible interpretations). Several authors found contradictory results showing an apparent enhancement of the velocity dispersion along the spiral arms (M 51; García-Burillo et al. 1993) or along the interarm regions (also in M 51; Rydbeck et al. 1991), both in the observations and in simulations of the same objects.

We will adopt here a distance to the galaxy of 20 Mpc (Van der Bergh 1989). At this distance $10'' \approx 1$ kpc. We take as the projection angles $i=32^\circ$ (the inclination angle) and PA=155° (the position angle of the major axis). They correspond to a kind of average of the various values given in the litterature for the projection angles. However the value of the PA is somewhat uncertain (see discussion of Paper I).

All through this paper, we will denote by x and y axis the kinematical minor and major axis respectively.

Sections 3 and 4 describe, respectively, the Canzian test and its application to the NGC 4321 HI data cube (which is briefly presented in Section 2 together with the CO and H α maps). Section 5 is devoted to present the numerical simulation models, their results, and how they compare with the observations.

2. Observations: the CO, HI and H α data

In this section we intend to present briefly the ensemble of the observations used through the subsequent discussion.

NGC 4321 has been classified as an Sc galaxy by Sandage & Tamman (1987), but as SABbc by de Vaucouleurs et al. (1991) and it has a strong spiral wave in its disc. The near infrared image taken by Pierce (1986) completed this picture showing the existence of a prominent stellar bar that extends up to $R \approx 60''$, as well as an inner oval potential, within the inner $R \approx 15''$ and whose axis is slightly misaligned with the main bar. It is the brightest member of the Virgo cluster and possesses no strong visible companion nearby, apart from a NW dwarf that could be at the origin of a tidal perturbation detected in the HI map of Knapen et al. (1993).

CO was first observed by Young et al. (1985), Kenney & Young (1988) and Cepa et al. (1992), using single dish telescopes, as well as by Canzian (1989) using the OVRO interferometer in a 65'' field centered in the galaxy nucleus. Except for the high resolution map of Cepa et al. (1992) (made with a

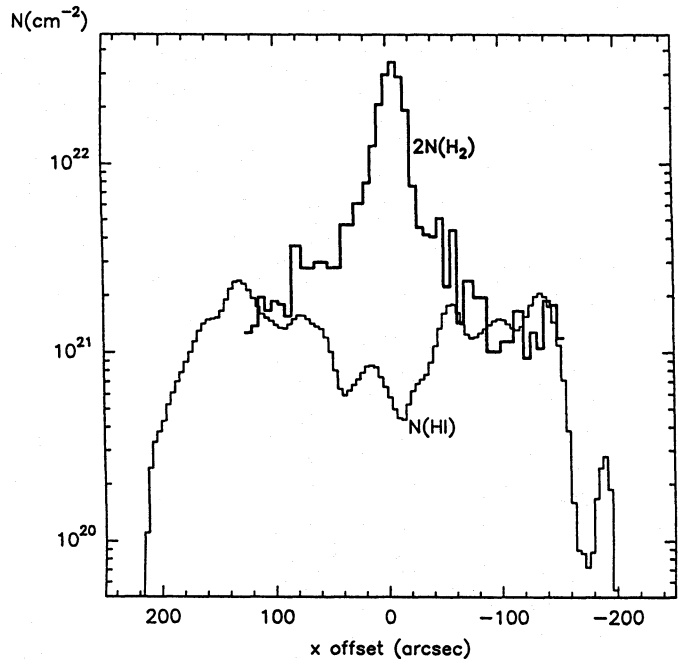


Fig. 1. We show the average HI and H₂ column densities for a strip parallel to the minor axis, obtained by averaging in the y direction ($\Delta y = 20''$), as a function of the x offset in arcsec

spatial resolving power of 14''), that covered partially a spiral arm and one of its neighbouring interarm regions, the previous single-dish surveys were unable to furnish a detailed picture of the distribution and kinematics of molecular gas. The interferometer map of Canzian concerns only the galaxy centre (up to $R \approx 40''$). It reports the detection of a complex structure consisting of 5 molecular gas complexes: one at the radiocontinuum centre and the other four forming a ring-like structure that has its counterpart in the H α map (see discussion below).

Our CO high resolution observations of NGC 4321 have been extensively described in Paper I. As we were searching for the kinematical signature of the corotation resonance, we completed a partial map in the 2 \rightarrow 1 and 1 \rightarrow 0 transitions of ¹²CO restricted to cover the minor axis (the reversal of the radial streaming motions should be directly detectable since the tangential component of these motions is zero along the minor axis). The CO map extends up to a radius $R \approx 180''$. The absence of sign change on the radial streaming motions visible in the position-velocity diagramme taken along the kinematical minor axis led us to conclude that the corotation circle lies at the outer disc ($R \geq 160''$).

We also mapped two selected square regions centered on what Elmegreen et al. (1989) identified as the 4:1 resonances in the enhanced optical pictures of NGC 4321. It is expected from the theory that arm-interarm contrasts and streaming motions are particularly strong in the vicinity of the 4:1 resonances: the gas flow is more strongly perturbed as the pitch angle of these interarm spurs is larger than that of “normal” spiral arms. However, we detected no morphological or kinematic signature of these resonances in the CO data. The CO line-widths are not

abnormally large either (the beam smearing in our observations might cause a widening of the observed lines if there was a strong non-resolved velocity gradient within the 12''(and 21'') beam caused by the expected strong streaming motions).

The HI content and kinematics of NGC 4321 were studied by Warmels (1988), and Cayatte et al. (1990) at 45''resolution and by Knapen et al. (1993) using the VLA array at C and D configurations (resolutions in the final data cubes between 13'' and 45''). In the HI maps of Knapen et al. (1993), the neutral atomic component is detected over the whole disc of the galaxy. The distribution shows concentrations over the main spiral arms, and a relative deficiency in the centre which corresponds to the peak emission of CO. This effect has been observed in many galaxies (see Young & Scoville 1991). Over most of the disc, HI is limited to the radial extent of the optical disc, except for a large but faint extension detected on the SW side of the galaxy in the 45''resolution data. Deviations from circular motions were found in this same SW area, over the spiral arms (due to streaming motions) and in the central parts of the galaxy (due to gas streaming around the bar). The position-velocity diagram taken along the minor axis reveals the main features also present in the CO observations (see Paper I).

NGC 4321 was first completely mapped in H α by Arsenault (1990) at a resolution of 1.5''. In a previous paper, Arsenault et al. (1988) reported the existence of a complex nuclear ring of star formation and obtained the velocity field of the galaxy, which clearly shows the streaming motions associated with the crossing of the arms and a central S-shape distortion of the isovelocity contours along the bar axis. Cepa & Beckman (1990) and Knapen (1992), carried out high quality observations with a resolution of $\sim 1''$, covering the whole star forming disc of NGC 4321. Their images show weak H α emission from the bar region, enhanced star formation at the ends of the bar, and a non-symmetric distribution of HII regions in the disc of the galaxy. The strongly emitting nuclear part of the galaxy (16% of the total H α luminosity of the disc) shows a patchy distribution that has been also reported by Canzian (1989). This structure is reproduced as well in the CO interferometer observations and has been interpreted as a possible four-armed spiral structure, probably related with the two Inner Lindblad Resonances (ILR).

3. The Canzian test

The test proposed by Canzian (1993) is based on the study of the morphology of residual velocity maps in spiral galaxies, obtained from the field of measured radial velocities, once the contribution from rotation has been subtracted. The corotation radius defines the boundary between two regions of different morphology. Inside the corotation region, we have one pair of approaching (blueshifted velocities)-receding (redshifted velocities) spiral arms. Outside corotation, this m=1 morphology changes to a m=3 morphology (three pairs of approaching-receding spiral arms).

This effect can be easily explained if we analyse the functional form for transonic solutions of the radial velocity pertur-

bation field of a fluid in a galaxy disc where an "external" spiral potential is present (see Shu et al. 1973, for details). Assuming that we are inside corotation, the observed radial velocity (without rotation), V_{rad} , corresponding to the gas flow in an inclined spiral galaxy disc has the following functional dependence:

$$V_{rad} \sim \sin(\theta - \alpha)\sin(i) \quad (1)$$

where θ is the angle from the line of nodes, α the spiral arm pitch angle and i is the inclination of the galaxy disc. The dependence of V_{rad} on $\sin(\theta)$ implies that we have one pair of receding-approaching spiral arms.

Outside corotation, this functional dependence on θ becomes:

$$V_{rad} \sim \sin(3\theta - \alpha)\sin(i) \quad (2)$$

Now the $\sin(3\theta)$ term shapes the V_{rad} field into a three paired receding-approaching spiral arm morphology.

As it is discussed by Canzian (1993), this change of morphology is independent of the exact mathematical dependence of the velocity perturbations induced by the spiral potential (in this case we have supposed a sinusoidal field) and it is entirely due to the change of sign of the gas streaming motions beyond the corotation circle, affecting only the radial component and not their tangential counterpart (see Fig. 2 of Canzian 1993).

In practice, the application of this method to identify the position of the corotation resonance may encounter some difficulties and therefore its results should be taken with caution.

First of all, the knowledge of the rotation curve seems crucial: the related change of morphology in the residual velocity map can be somewhat masked if the rotation curve is not properly subtracted. On the other hand, we have implicitly assumed that the spiral arm pitch angle is constant and so independent of θ . This is far from being the case in "real" spiral galaxies where the spiral arm morphology can be severely distorted (for example by the presence of a bar or through a close encounter with a companion galaxy). In particular, Canzian (1993) suggested that the case of NGC 4321 could be problematic for applying his method, due to the existence of possible interacting companions and its non-symmetric rotation curve. Even if the main bar of NGC4321 distorts the velocity field and produces an extended corotation region, we have considered this galaxy to be an appropriate candidate to apply the 2-D test because the presence of the bar ensures the existence of a well defined main wave mode characterized by Ω_p and associated with both the bar and the spiral arms.

To better compare with NGC4321, we will study by means of an analytical model the combined effect of a bar plus spiral potential on the residual velocity field obtained in the Canzian test.

Velocities of the gas in this model are computed following Shu et al. (1973), for a slightly nonlinear regime of the gas. The perturbed gravitational potential is given by a bar perpendicular to the minor axis, in the inner 6 kpc radius, and by a logarithmic spiral of pitch angle 15° in the rest of the galaxy disc. The OLR bounds the outer edge of the model at a radius of 18 kpc. The

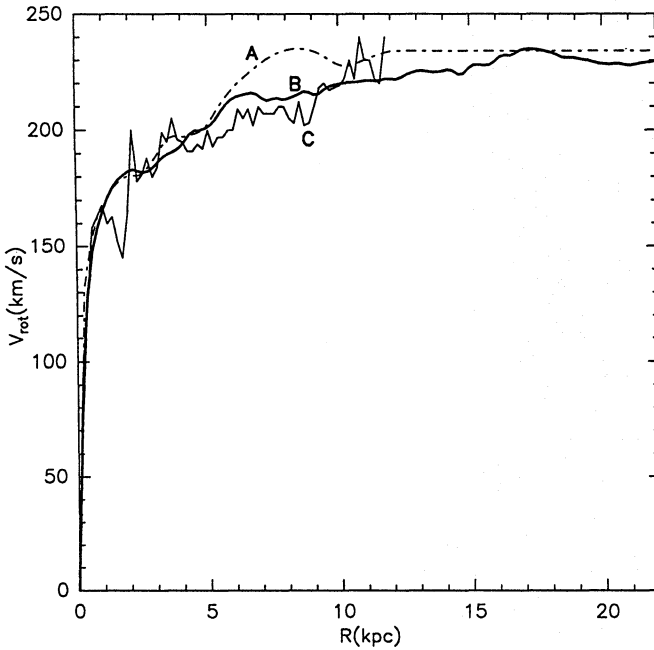


Fig. 2. We show the comparison of the rotation curves in NGC 4321 as derived from H α data by Arsenault et al. (1988) (c), from the HI map of Knapen et al. (1993) (a) and labelled by (b) we present the rotation curve finally adopted in the numerical simulations

shape and intensity of the perturbation agrees fairly well with that of the real galaxy.

We have used for our purpose the rotation curve obtained from the numerical simulations and an $\Omega_p = 20 \text{ km s}^{-1} \text{kpc}^{-1}$ that places corotation at a radius of $R_{CR} = 11 \text{ kpc}$.

As expected (see Fig. 3a), after subtraction of the rotation curve from the theoretical velocity field, we can see in the inner corotation region one pair of approaching-receding parts showing the inner barred structure (I1a, I1r). In the region outside corotation we have three pairs of approaching-receding spiral arms.

Note that the position of the three pairs of spiral arms is related to the spiral potential: there is a pair that crosses over the spiral potential and it is a prolongation of the inner pair structure (O1a, O1r). The two others pairs begin to diverge from the inner pair at a radius of 8 kpc and the transition finish at the corotation ellipse. The first trails (O2a, O2r) and the second (O3a, O3r) leads the spiral potential. We draw attention to the effect of the bar: the inner velocity field is strongly distorted and the transition region or “corotation zone” extends from 8 kpc to 11 kpc.

We discuss in the next section the practical application of the Canzian test to the HI data cube and to the simulations in NGC 4321, used as a diagnostic to identify the corotation resonance in this galaxy and compare its results with the conclusions derived from the model and the CO map of Paper I.

4. Results of the Canzian test

We have applied the “phase method” proposed by Canzian to the velocity field extracted from the HI 20'' resolution image of Knapen et al. (1993). In the 20'' map, the streaming motions driven by the spiral wave and affecting the gas in the inter-arm and arm regions are resolved. Moreover, this choice for the equivalent angular resolution appears as a good compromise as it optimizes the final signal to noise ratio on the map (the 15'' data set is too noisy while in the 45'' map any signature of streaming motions are completely smeared out).

Even if the atomic gas is largely deficient within the inner 6 kpc (see Fig. 1 for comparison with molecular gas distribution), we can notice a strong distortion in the HI velocity field within the inner 9 kpc driven by the stellar bar (see Knapen et al. 1993). Such a bar-driven distortion in the velocity field is clearly visible in the CO position-velocity minor axis diagram discussed in Paper I.

At a first step, we subtract the rotation curve from the HI velocity field. The rotation curve in NGC 4321 has been derived by several authors using different tracers of the gas (H α : Arsenault et al. 1988; HI: Guhathakurta et al. 1988, Knapen et al. 1993; optical spectra: Rubin et al. 1980). The agreement between these various determinations is satisfactory up to a distance of $R \sim 150''$. Knapen et al. (1993) and Guhathakurta et al. (1988) report the existence of two different rotation curves in the North and the South sides of the HI gas disc from $R \sim 150''$ outwards. They interpret the scatter as a signature of strong z motions affecting the HI gas disc owing to tidal forces induced by NGC 4322 or as a result of a self-sustained warp in the outer disc. The real rotation curve in the outer parts is therefore somewhat uncertain. As the scenario where we apply the Canzian test (the 20''HI gas disc) has a maximum radial extent of $R \sim 150''$, we have finally adopted a flat rotation curve in the outer region (see Fig. 2)

There are other factors limiting the efficiency of the phase method in giving a clear answer in the case of real galaxies: an accurate determination of both the dynamical centre and the systemic velocity (v_{sys}) of the galaxy is crucial. A displacement of the dynamical centre causes a misalignment of the computed theoretical velocity field from the observed one that can invalidate the phase method. On the other hand the residual velocity pattern changes depending on the systemic velocity assumed for the object. If we subtract an overestimated (underestimated) value of v_{sys} to the radial velocity field, the total disc area with approaching (receding) velocities is too large. Nevertheless, we believe that such uncertainties are kept reasonably low in our case. From the CO data taken at the centre (see Paper I), we determine a value for the dynamical centre in good agreement with the one derived from the HI map (within an error of less than 2''). Furthermore, the determination of the systemic velocity of NGC 4321 has been improved by several authors in recent years (see Warmels 1988; Guhathakurta et al. 1988; Cepa et al. 1992).

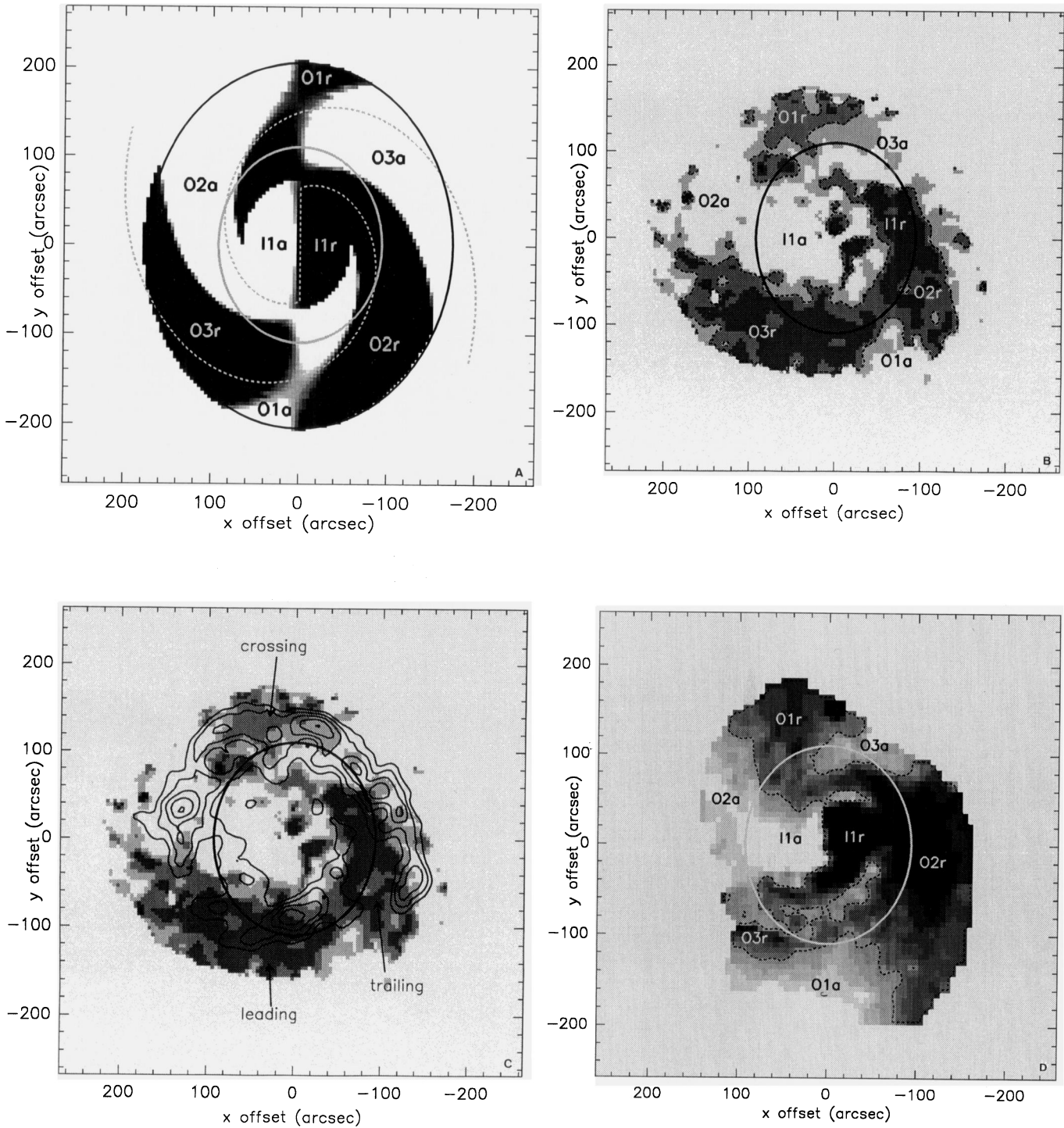


Fig. 3. **a** shows the modelled velocity field due to a density wave. The perturbed bar plus spiral potential is displayed as a dashed curve. In **b**, the residual velocity field obtained after subtraction of the rotation curve to the observations. **c**, the same as **b** with an overlay of the HI isodensity contours of the arms to show the location of the three outer approaching-receding spirals in relation to the spiral potential. **d** shows the result of the Canzian test from the best fit of the simulations $\Omega_p = 20 \text{ km s}^{-1} \text{ kpc}^{-1}$. The ellipse represents in all the cases the expected position of the corotation circle for $\Omega_p = 20 \text{ km s}^{-1} \text{ kpc}^{-1}$. The line-of-sight radial velocities are represented by lighter shades for negative (approaching) velocities and darker shades for positive (receding) velocities. The scale range saturates at -10 km/s and 10 km/s

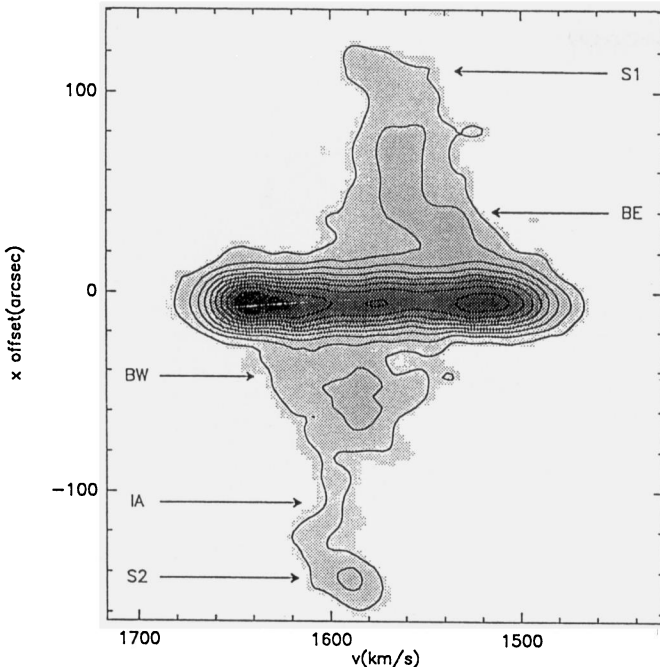


Fig. 4. Position-velocity diagram in $^{12}\text{CO}(1-0)$ taken along the minor axis of NGC 4321. The approaching (left side) and receding (right side) parts correspond to I1a-O2a (white) and I1r-O2r (black) of Fig. 3., respectively

Figure 3 shows the results of applying the Canzian test to the model of Shu et al. (a), to the 20'' HI data cube, (b) and (c), and to the best fit of the simulations, (d).

We clearly see the spiral-like pattern (the $m=3$ mode, i.e. three pairs of approaching-receding “spiral arm-like” regions) in the residual velocity field of the outer disc (outside corotation) that changes towards a $m=1$ mode pattern in the inner disc (inside corotation). This change of morphology does not occur at a “well” defined radius but there is a transition region with a certain extent ($R_{CR} = 8 - 11$ kpc). The reason behind such uncertainty resides in the distortion driven by the main bar on the velocity field. In NGC 4321 corotation is a radially extended region.

Nevertheless, the presence of the outer $m=3$ mode can be clearly assessed for the HI, the simulations and the analytical model, meaning that the spiral structure develops outside corotation. The outer morphology of the velocity field proves that we have crossed the “corotation region”.

Due to the deficiency of HI in the inner 6 kpc, we can hardly see the $m=1$ inner mode in the observations but we can complete this lack of information with our CO data taken along the minor axis which cover a part of this central region.

In Fig. 4 the approaching (right side) and receding (left side) parts visible in the $^{12}\text{CO}(1-0)$ position-velocity diagram taken along the minor axis correspond respectively to the white and black parts in the analytical model. The Z shape of the P-V diagram stands clear now as the distortion due to the main bar (see Paper I).

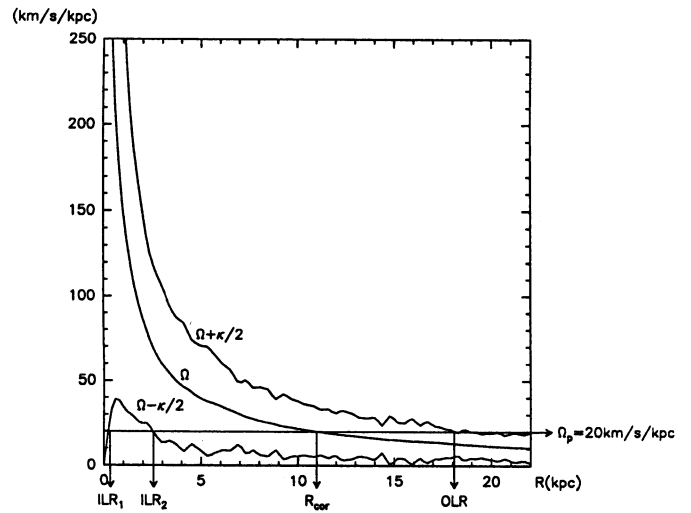


Fig. 5. The Ω , $\Omega - \kappa/2$ and $\Omega + \kappa/2$ curves for NGC 4321. The expected position of the resonances for $\Omega_p = 20 \text{ km s}^{-1} \text{ kpc}^{-1}$ are indicated by ILR_1 ($R = 0.4$ kpc) and ILR_2 ($R = 2.5$ kpc) (two Inner Linblad Resonances), $R_{CR} = 11$ kpc (corotation circle), and $OLR = 18$ kpc (Outer Linblad Resonance)

The three outer spiral arm pairs seen in the HI velocity field are situated at the expected sites of the galaxy disc with respect to the minima of the spiral potential as expected by the model (see Fig. 3a and 3c).

In the simulations of the molecular component the behaviour of the gas in the region inside corotation slightly differs from the model (see Fig. 3d): two faint white streaks between 3 and 8 kpc, almost parallel to the minor axis, can be seen inside corotation. These features correspond to the distortion of the central velocity field due to the orientation change of the orbits which precess progressively to follow the main bar (see Sect. 5). The similarity of both the simulation (Fig. 3d) and the model (Fig. 3a) in the inner 3 kpc is due to the fact that the small bar or oval potential in the real galaxy is oriented as in the model, perpendicular to the minor axis.

The application of the Canzian method to NGC 4321 provides an accurate estimate for the corotation in comparison with other observational methods. In the other hand, the Canzian test confirms the wave based-structure of this galaxy. Furthermore, the location of the corotation radius in the middle of the disc ($R_{CR} \simeq 11$ kpc), with a bar ending before corotation and the spiral arms crossing over the corotation region without discontinuity, could clarify the nature of the wave (either a mode or a shearing wave) and which of the different interpretations of the DWT developed in recent years is the most appropriate to explain the spiral structure of NGC 4321.

In recent N-body simulations, Combes & Elmegreen (1993) have proposed that the pattern speed of the bars depends essentially on their mass concentration: bars end at their corotation only in galaxies with a sufficient mass concentration (early-types in general). The bar pattern speed is related to the precession rates of orbits, represented in nearly axisymmetric discs by $\Omega - \kappa/2$. Early-type galaxies have large maxima of $\Omega - \kappa/2$,

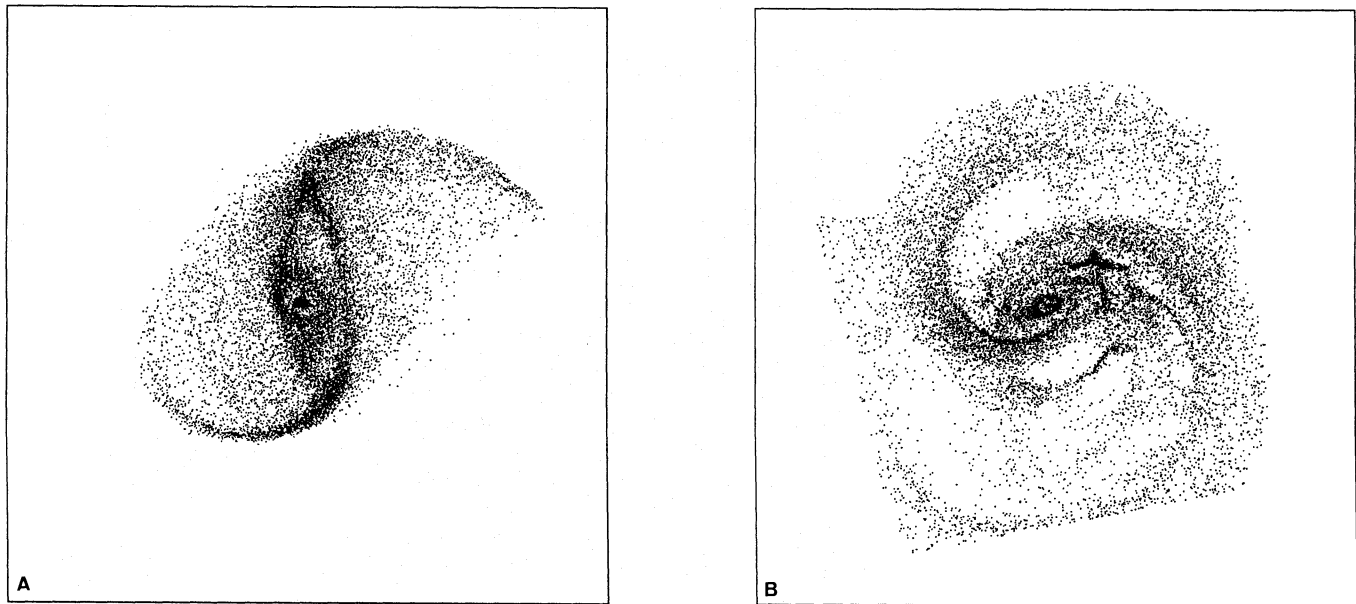


Fig. 6a and b. Particle plots of the molecular cloud distribution for two extreme values of Ω_p : **a** $\Omega_p=5 \text{ km s}^{-1} \text{ kpc}^{-1}$ and **b** $\Omega_p=35 \text{ km s}^{-1} \text{ kpc}^{-1}$. No coherent bar or spiral structure is obtained

and therefore high pattern speeds, such that corotation is well inside the stellar disc, at a small radius. The bars then extend almost towards corotation. In late-type galaxies, $\Omega - \kappa/2$ is everywhere very low, with no sharp maximum. The bar pattern speed is then much lower, and the corotation is pushed out to such a large radius that it occurs outside several exponential scale lengths. This prevents late-type bars from growing much larger after they form, since there are too few stars near corotation to absorb angular momentum. The bar is then limited by about the exponential disc scale length, which is where most of the disc mass is.

NGC 4321 has been classified SABbc, or Sc, and is of rather late-type. Its mass distribution is nevertheless sufficiently concentrated to display a marked maximum of the $\Omega - \kappa/2$ curve (see Fig. 5). We can then predict, assuming that the pattern speed is close to this maximum value, that the corotation will be well within the disc. We also expect the existence of an inner Lindblad resonance, as in mass-concentrated galaxy models. The pattern speed value that we find here by several methods is consistent with these expectations.

5. Computer simulations

5.1. Introduction

We have performed numerical simulations intended to study the evolution of the molecular gas disc of NGC 4321, under the influence of the spiral plus bar gravitational potential created by the old stellar disc. The gas disc is modelled as an ensemble of molecular clouds and the spiral potential is derived from the luminosity of a red CCD image. The stellar mass distribution, and consequently the potential extracted from it, is intended to be as close as possible to reality. The aim of this run of numer-

ical simulations is twofold: first of all, we try to fit the value of the pattern speed of the spiral wave in the disc by studying the different gas responses varying this critical parameter. The value of Ω_p provides an estimation of the corotation radius that can now be compared and criticized with the various observational determinations. Once the fit is judged satisfactory, we can shed light on different aspects of molecular cloud dynamics, by studying the gas arm-interarm contrast, streaming motions and velocity dispersion maps in the “simulated” galaxy.

5.2. Determination of the gravitational potential and the rotation curve

We first derive the gravitational potential that will be used in the simulations. We chose a fair tracer of the old stellar population (a red broad band CCD image of NGC 4321) in order to derive the total mass distribution with a minimum number of hypotheses concerning the radial variation of the M/L ratio. The red CCD image was obtained in the Roque de los Muchachos Observatory at La Palma, with a filter of bandwidth 15Å, centred at 6565Å. The spatial resolution is close to 0.8''.

The red image is deprojected onto the plane of the galaxy, assuming an orientation of PA (position angle)=155° and i (inclination angle)=32°. The brightness distribution in the plane of the galaxy is converted into mass distribution via an arbitrary preliminary M/L ratio. Then we derive the gravitational potential from the Poisson equation using a fast Fourier transform method on a grid of 256x256 pixels of 1''x1'' size. At this point we start fitting the radial profile of the M/L ratio. Comparison of the thus computed rotation curve with the observed ones requires a modification of the M/L ratio as a function of radius, especially in the inner 6 kpc radius. This divergence between modelled and observed rotation curves is partially due to a slight

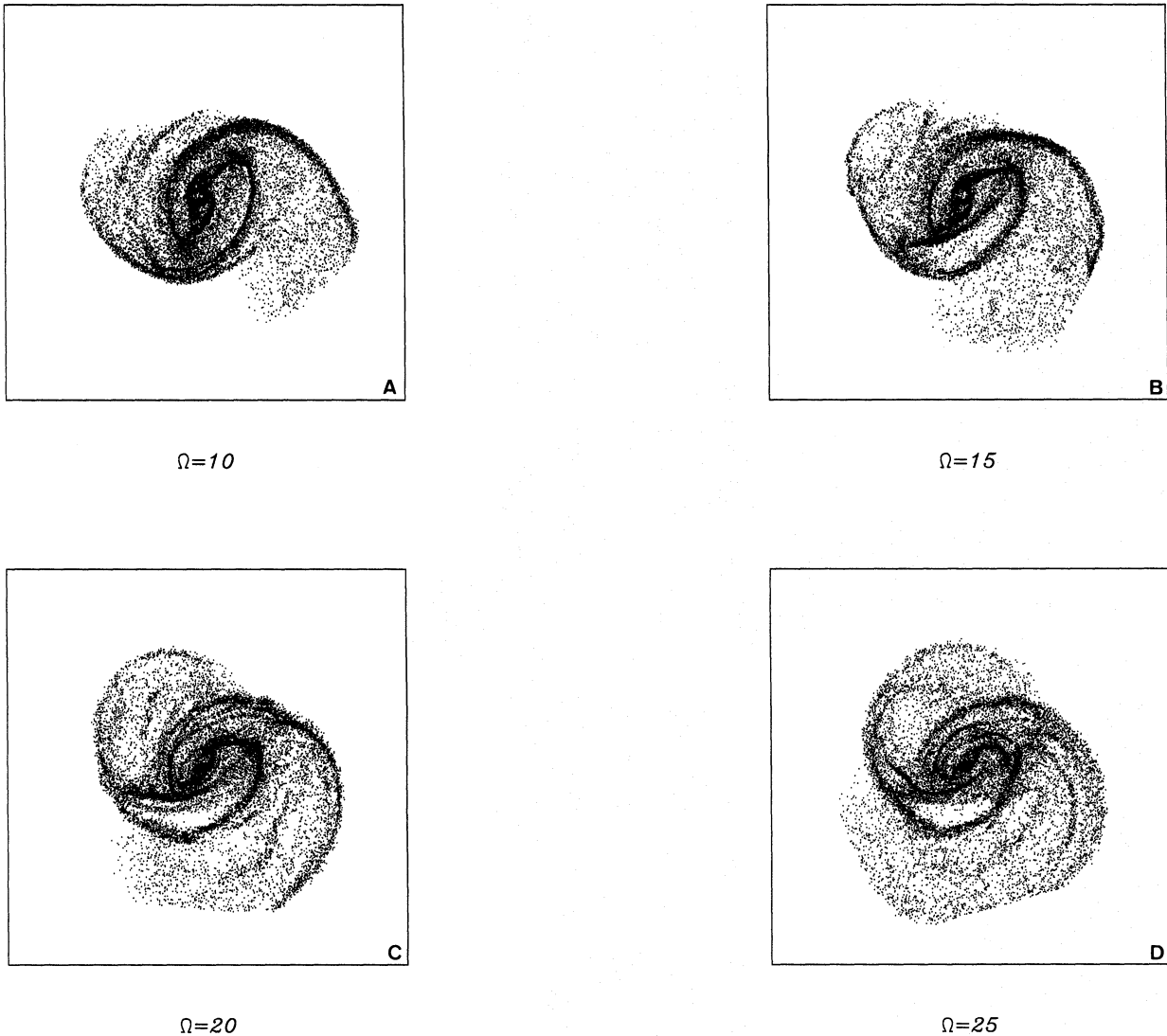


Fig. 7a–d. Particle plots showing the distribution of molecular clouds in the NGC 4321 disc (plane of the galaxy) for several simulation runs corresponding to different trial values of Ω_p : **a** $\Omega_p = 10 \text{ km s}^{-1} \text{ kpc}^{-1}$, **b** $\Omega_p = 15 \text{ km s}^{-1} \text{ kpc}^{-1}$, **c** $\Omega_p = 20 \text{ km s}^{-1} \text{ kpc}^{-1}$, the best fit, and **d** $\Omega_p = 25 \text{ km s}^{-1} \text{ kpc}^{-1}$

saturation of the red image in the central parts, and to extinction due to dust in the inner ~ 2 kpc, associated with a region of enhanced star formation. In the process, we add a small spherical bulge of mass $5 \cdot 10^9 M_\odot$ and radius 0.7 kpc.

We finally adopt a rotation curve for the simulations (see Fig. 2) which is nearly flat from $R \sim 150''$ up to $R \sim 250''$ (corresponding to the edge of the disc in the simulations), a reasonable assumption in view of the general trend of the observed rotation curves for spiral galaxies.

The red image reveals the outstanding features of the mass distribution in the disc: the two arm spiral structure stretches out from a stellar oval whose detection was already reported by Pierce (1986). The inner central region has been recently resolved in H α (Cepa & Beckman 1990; Canzian 1992) and in CO observations (Canzian 1992), showing the presence of an inner four-armed spiral structure associated with the inner

oval. Probably because of a lower spatial resolution, Arsenault et al. (1988) failed to resolve the inner spiral arms and instead they reported the identification of an inner ring of star formation encircling the small oval feature. Both are right, since the ring is made from the winding end of the spiral arms at that radius.

The origin of this complex morphology of stars and gas near the centre could be related to the existence of another mode, faster than the main $m=2$ one (cf. Combes 1993).

We follow the evolution of molecular clouds in 3 dimensions so we have to extend the gravitational potential in the z direction (perpendicular to the galaxy plane). For the sake of simplicity we assume cylindrical symmetry, thus the gravitational forces in the plane (F_x and F_y forces) are independent of z . This approximation seems largely justified as the molecular gas disc is much thinner than the stellar plane ($z_{gas} \sim 50\text{pc}$

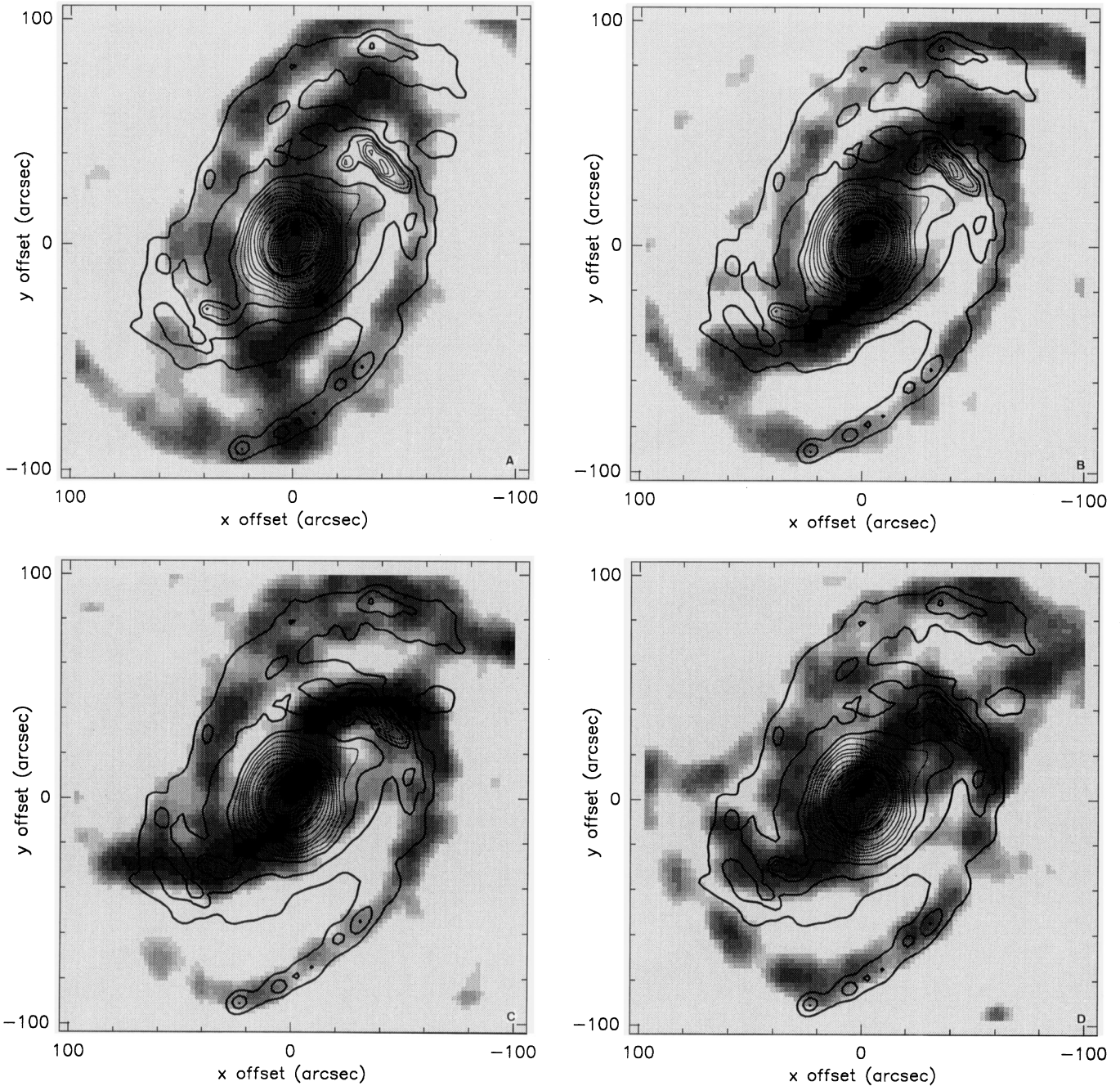


Fig. 8a-d. Superposition of the “observed” density gas distribution in the simulated galaxy (grey scale) with the red image (solid contours) in the inner 10 kpc, for the tested values of Ω_p : **a** $\Omega_p=10 \text{ km s}^{-1} \text{ kpc}^{-1}$, **b** $\Omega_p=15 \text{ km s}^{-1} \text{ kpc}^{-1}$, **c** $\Omega_p=20 \text{ km s}^{-1} \text{ kpc}^{-1}$, the best fit, and **d** $\Omega_p=25 \text{ km s}^{-1} \text{ kpc}^{-1}$

and $z_{stars} \sim 2 \text{ kpc}$). The percentage of molecular clouds that escapes from the plane into the halo is always negligible.

The vertical z-forces are derived assuming that the stellar plane obeys the equilibrium of an infinite layer with a density law $\rho = \rho_0 \operatorname{sech}^2(z/H)$, where H is the scale-height; we have taken $H = 2 \text{ kpc}$.

The gravitational potential, intended to be the closest to the real potential field, includes the spiral arms and the stellar bar.

Moreover, the inner small stellar bar is also clearly visible in the red CCD image.

The next step consists of decomposing the total stellar potential into its axisymmetric and non-axisymmetric parts by making a two-component model fit. The axisymmetric part ($P_{ax}(r)$), representing most of the contribution from the stellar disc, is derived making an azimuthal average of the total potential ($P(\theta, r)$) for each radius:

$$P_{ax}(r) = \int_{2\pi} P(\theta, r) d\theta / \int_{2\pi} d\theta$$

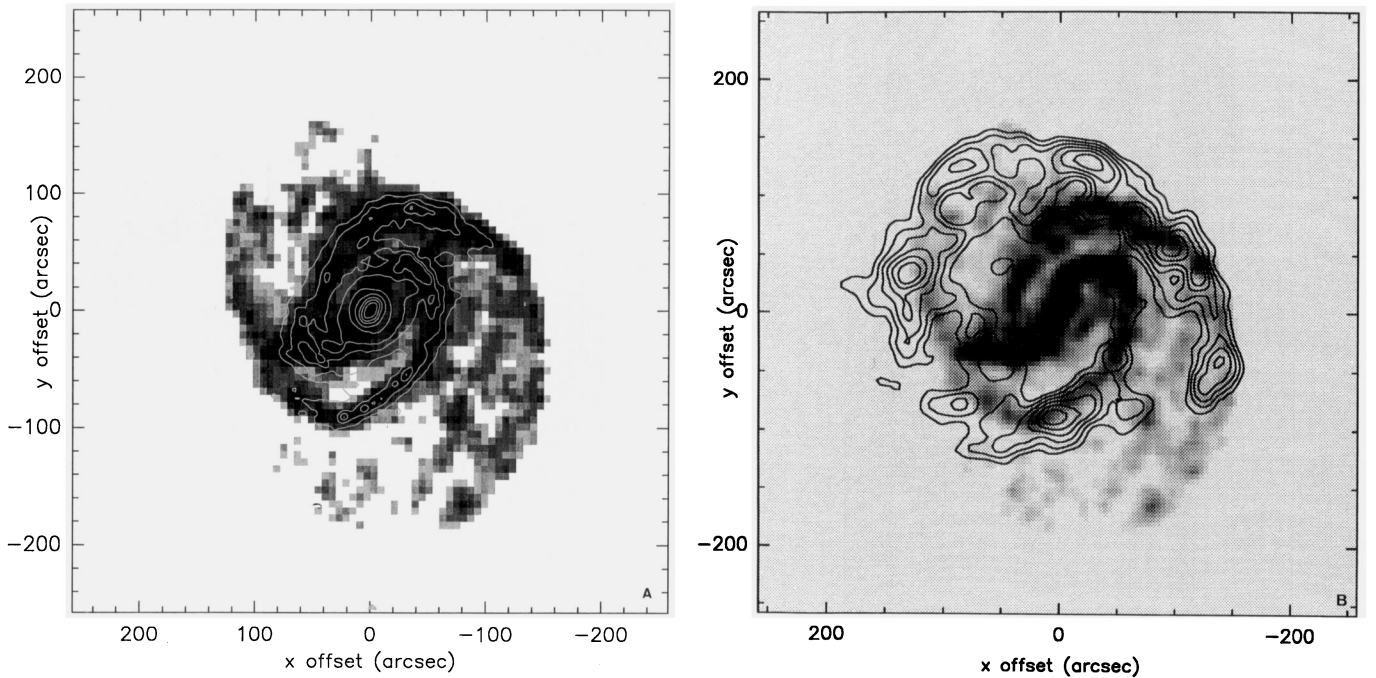


Fig. 9. **a** A close picture on the superposition of the simulated response of the gas disc (grey scale) and the red image (solid contours) used to derive the potential for $\Omega_p=20 \text{ km s}^{-1} \text{kpc}^{-1}$, the best fit. **b** The same as **a** but using the HI map (solid contours)

The derivation of the non-axisymmetric component is straightforward, being the difference:

$$P_{nonax}(\theta, r) = P(\theta, r) - P_{ax}(r)$$

At the beginning of each simulation, molecular clouds are launched in the axisymmetric gravitational potential. The non-axisymmetric part is introduced gradually with a certain time lag of the order of 20% the total simulation time (7.2×10^8 years).

If we introduced from the beginning of the simulation the spiral arm pattern with no delay, molecular clouds would fall rapidly towards the nucleus, being trapped in elliptical orbits and forming a molecular bar at the centre. This is what is expected from the evolution of a gaseous disc under the action of the gravitational torques exerted by a spiral plus bar wave pattern, in the long run. However such a rapid dynamical evolution for the gas disc is highly unrealistic and we have to suppose a certain time delay for the spiral structure to settle down in the stellar disc. Actually, spiral structure always appear gradually as shown by many self-gravitating 3-D simulations of stellar discs, whatever mechanism is invoked to explain its origin (the presence of a companion, the existence of a central stellar bar or the swing-amplifier mechanism).

Figure 2 shows the adopted rotation curve for the model. Fig. 5 presents the Ω , $\Omega - \kappa/2$ and $\Omega + \kappa/2$ curves, where κ represents the epicyclic frequency and Ω is the angular velocity.

5.3. Numerical models

We have carried out several runs of simulations with three different models to treat a variety of problems as the dissipation effects in the gas and the importance of the self-gravity in a

possible shift of the gas shock relative to the centre of the stellar potential.

In first and second models we consider molecular gas as a non self-gravitating component.

- In the first model the molecular gas disc is treated as an ensemble of homogeneous molecular clouds (density is constant) with masses ranging from $10^3 M_\odot$ to $10^6 M_\odot$. The parameters (mass and radius) that characterize the model clouds have been chosen within intervals similar to the ranges observed in the Galaxy. The clouds mass distribution is described by a power-law spectrum ($M \sim M^\alpha$) with an index $\alpha \sim -1.5$; therefore we assume a mass function similar to the one commonly adopted for our Galaxy (see Casoli & Combes 1982). Molecular clouds evolve under the external action of the gravitational potential of the stellar disc, acting as test particles.

Clouds interact with each other via inelastic collisions whose outcome can be coalescence, mass exchange or fragmentation. The details of the model are described in Combes & Gerin (1985); this collisional scheme has been used already in the study of the molecular cloud dynamics of the interacting system M 51 (see García-Burillo et al. 1993). A certain percentage of molecular clouds reach the top mass box-case corresponding to the giant molecular clouds (GMC's) ($M_{GMC} \sim 3 \times 10^5 M_\odot$), preferentially along the spiral arms where the cloud-cloud collision rates are markedly enhanced. After 4×10^7 years the GMC's are dispersed, simulating star formation events, and re-injecting energy and mass in the form of small clouds with an isotropic velocity dispersion of 10 km/s. In this way we try to simu-

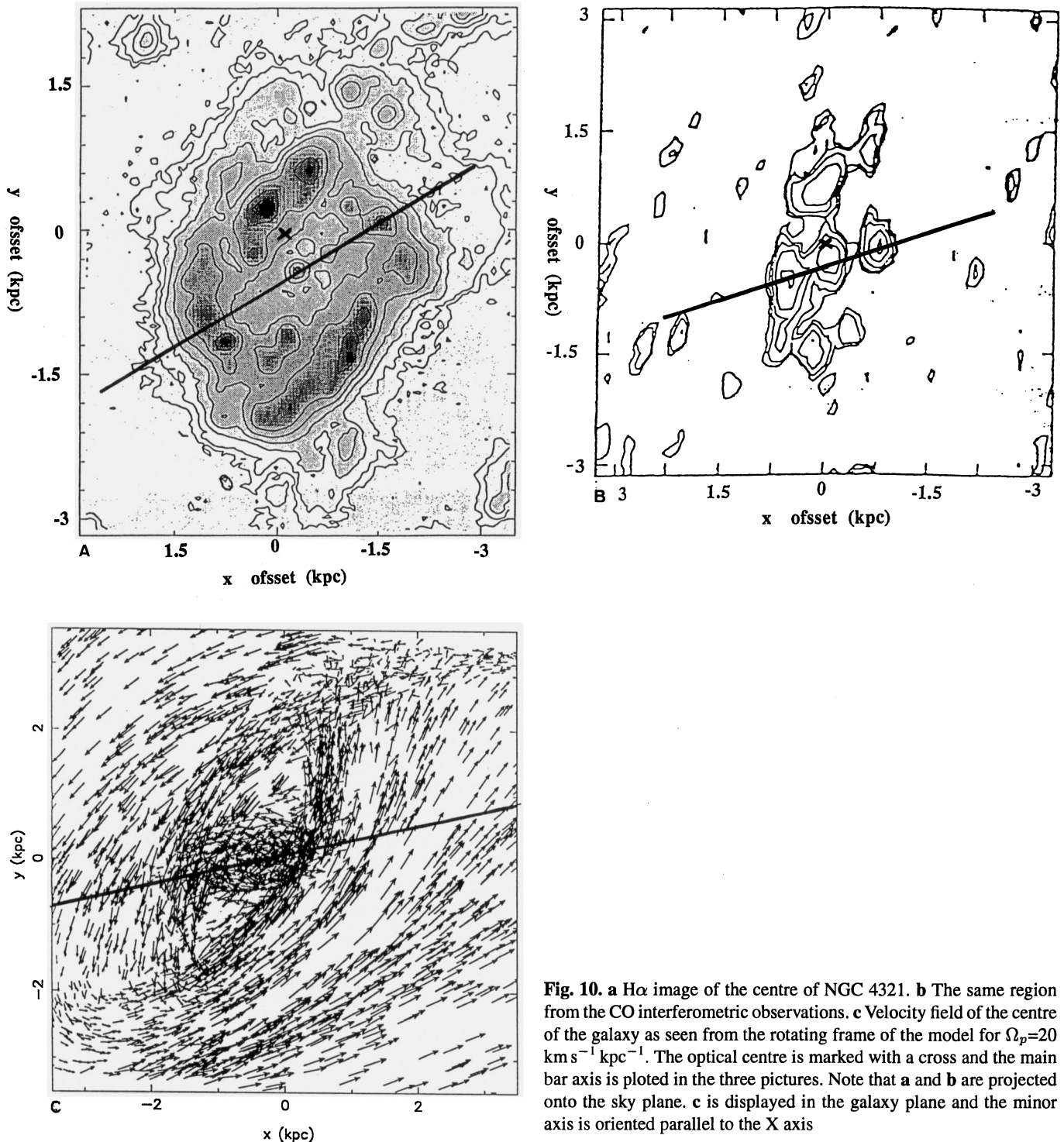


Fig. 10. **a** H α image of the centre of NGC 4321. **b** The same region from the CO interferometric observations. **c** Velocity field of the centre of the galaxy as seen from the rotating frame of the model for $\Omega_p=20$ km s $^{-1}$ kpc $^{-1}$. The optical centre is marked with a cross and the main bar axis is plotted in the three pictures. Note that **a** and **b** are projected onto the sky plane. **c** is displayed in the galaxy plane and the minor axis is oriented parallel to the X axis

late the influence of massive star formation on the molecular cloud dynamics: the energy dissipated in cloud-cloud collisions is balanced by the energy re-injected by SF events. The results of inelastic collisions will be employed for the comparison with the observations.

- In order to analyze the contribution of dissipation effects in the gas behaviour and to follow better the particle orbits in

the plane of the galaxy (especially in the centre) we also carried out simulations with partially inelastic collisions. In the second model, we adopt particles with the same mass, arbitrarily fixed to $10^3 M_\odot$. The inelasticity parameter is taken to be ~ 0.65 in the direction parallel to the relative velocity between two collision partners, and 1 in the direction perpendicular to the encounter, to assure the conservation of the angular momentum. We do not include the effect of

star formation events in the gas. In this manner, we can appreciate the contribution of dissipation effects in the gas behaviour in comparison with the first model.

We will use this second model in all the particle plots in the plane of the galaxy to improve the particle orbits.

- The third model try to test the role of the self gravity in the relative phase shift between the gaseous and stellar component, as the model fitting is based on the gas response to the stellar potential extracted from the red image. As in the second model we have carried out simulations with partially inelastic collisions. The gravitational forces due to the gas have been computed by an FFT method in cartesian coordinates with a 256x256 grid, as described by Combes et al. (1990), and added to the imposed stellar potential. The total mass of the molecular gas within 12 kpc radius is $7 \cdot 10^9 M_\odot$, i.e. 7% of the total mass (cf. Kenney & Young 1988).

In the three cases the collisional grid is two-dimensional, though the molecular cloud orbits are followed in 3 dimensions.

We have adopted an exponential law for the radial distribution of molecular clouds in the disc with a scale length $h=5$ kpc ($50''$) (Kenney & Young 1988; Cepa et al. 1992). Alternatively we could have adopted the radial distribution of molecular gas along the minor axis taken from our observations that show a CO source strongly peaked towards the nucleus. If we adopt this radial distribution for the beginning of the simulations, the number of particles at the outer disc is dramatically reduced and our chances to get a detailed picture of the gas kinematics far from the centre become consequently hazardous.

The expected dynamical evolution for the gas, whenever spiral structure is present in the disc, involves inward radial transport phenomena that can explain the apparent CO radial distribution of some spiral galaxies. We can conclude that the real radial distribution of the gas when the spiral structure just starts to develop is probably much less centrally concentrated than it is shown in the CO measurements. Therefore, our choice for the initial radial distribution of molecular gas seems largely justified.

At the starting point for the simulations, molecular clouds are launched in equilibrium with $P_{ax}(r)$ and with a small velocity dispersion of 10 km/s.

5.4. Model fitting

The model fitting procedure relies on the precision with which we can estimate the optimum value of Ω_p in the disc of NGC 4321. The gas response is very sensitive to this parameter.

First we compute, for each trial value of Ω_p , a data cube for the simulated galaxy. We use the positions and radial velocities of each cloud at the final time of the simulations. To better compare simulations and observations we use a convolution beam of $12''$ (FWHM) to “observe” the simulated galaxy. The CO map being restricted to the vicinity of the kinematical minor axis region, we employed a combined data set of gas (HI and H α) plus red image which covers the entire disc in order to get a sensible global fit.

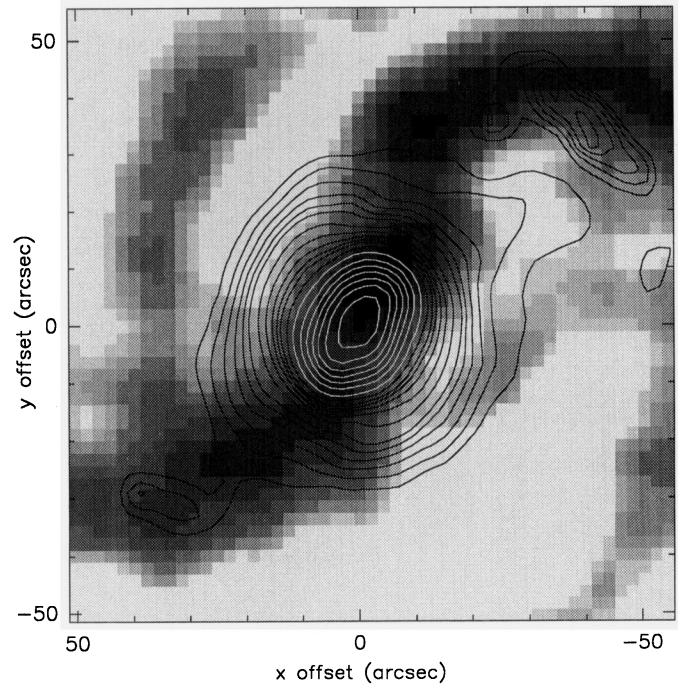


Fig. 11. Overlay of the density gas distribution for the best fit of the simulations (grey scale) on the real potential of the galaxy (solid contours) in the inner 5 kpc. Molecular gas response is leading from the gravitational potential minimum

In the inner disc, where HI is largely deficient, we need to use the information from the potential (particularly the gas response to the main stellar bar), and from the H α and CO interferometric images in the inner 3 kpc radius. At the outer disc, where spiral arms are beautifully delineated in HI, we use this tracer of neutral gas to compare with the simulated gas response. We will fit the simulations on the observed gas distribution and therefore determine Ω_p . We can reasonably discard an acceptable solution having a value of Ω_p outside a restricted range ($\Omega_p = 10 - 25 \text{ km s}^{-1} \text{ kpc}^{-1}$), as the final morphologies obtained for those values depart notably from the observed gas response. For Ω_p 's not belonging to the interval, no coherent bar and spiral structure in the gas component is obtained. Figure 6 illustrates two of these extreme cases for $\Omega_p=5$ and $35 \text{ km s}^{-1} \text{ kpc}^{-1}$. The gas morphology obtained clearly differs from NGC 4321. In Fig. 6a the bar occupies the entire disc of the galaxy and is perpendicular to the real potential. In Fig. 6b the spiral arms have almost disappeared.

Figure 7 shows the final configurations of the molecular gas disc for the completed simulation runs of the second model with four different values of $\Omega_p = 10, 15, 20$ and $25 \text{ km s}^{-1} \text{ kpc}^{-1}$. Depending on the value of Ω_p , the gas response to the potential evolves differently with time. In particular, for the extreme values of $\Omega_p=10$ and $25 \text{ km s}^{-1} \text{ kpc}^{-1}$, the spiral structure response to the potential disappears entirely after 2 rotation periods. This can be taken as a clue of what range of parameters give a sensible response of the gas to the spiral potential.

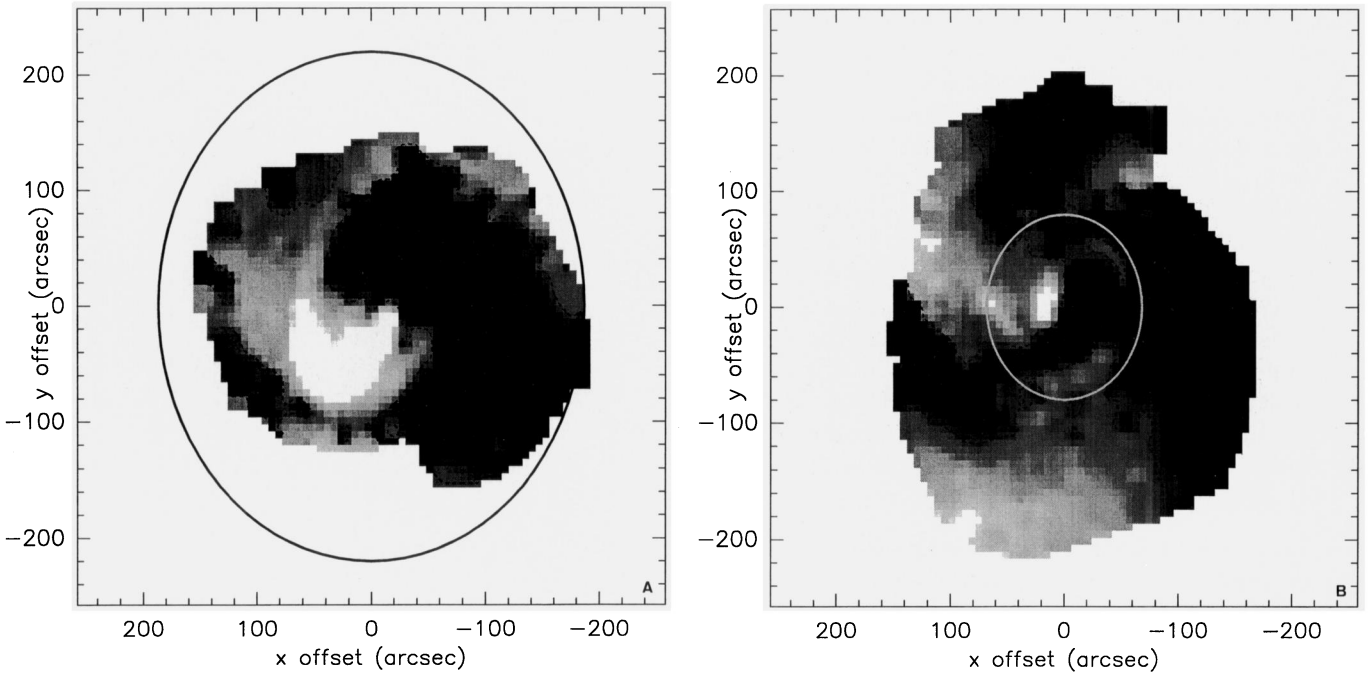


Fig. 12a and b. The Canzian test applied to the simulation data cubes for two different Ω_p 's: **a** $\Omega_p = 10 \text{ km s}^{-1} \text{kpc}^{-1}$, **b** $\Omega_p = 25 \text{ km s}^{-1} \text{kpc}^{-1}$

Figure 8 shows the overlay in the inner 10 kpc of the minimum of the potential (delineated by the isodensity contours of the red image) on the modelled intensity map obtained from the first model (grey scale) for $\Omega_p = 10, 15, 20$ and $25 \text{ km s}^{-1} \text{kpc}^{-1}$. Two spiral arms stretching out from a bar appear in all the simulated maps as observed in the optical image. The relative position between the gaseous and the stellar bar plus spiral structure changes rapidly with the adopted Ω_p : the bar plus spiral gaseous structure pivots in advance of the potential as Ω_p decreases.

This result can be easily interpreted: periodic orbits change its orientation by 90 degrees when they cross over a resonance. For low Ω_p the location of the corotation moves at the edge of the disc and the gaseous structure precesses more slowly. For high Ω_p , corotation moves closer to the centre, and the gas streaming is influenced by the perpendicular periodic orbits outside corotation. For this reason extreme values of Ω_p give no coherent structures.

The angular pattern speed Ω_p , plotted as a horizontal line in Fig. 5 gives an indication of the different corotation radius for each model which varies from $CR = 22 \text{ kpc}$ for $\Omega_p=10$ to $CR=8 \text{ kpc}$ for $\Omega_p=25 \text{ km s}^{-1} \text{kpc}^{-1}$.

Taking into account that the gas bar response and the main stellar bar should be in phase (following the x_1 orbits) and that the simulated gaseous spiral structure should also coincide with what we see in the response of the HI gas, the best agreement between the observations and the simulations is obtained for $\Omega_p = 20 \text{ km s}^{-1} \text{kpc}^{-1}$. In Fig. 9 we shows an overlay of the simulated gas response for the best fit (grey scale) on (a) the red image and(b) the HI observations: simulated bar and spiral potential closely follow the observed structure.

For our best fit-model ($\Omega_p = 20 \text{ km s}^{-1} \text{kpc}^{-1}$), the corotation radius is $CR = 11 \text{ kpc} (=110'')$ midway between the centre and the outer disc edge. This result is in excellent agreement with the value estimated by Elmegreen et al. (1989) from the identification of optical features of density wave resonances, as well as with the result obtained from the Canzian test applied to the HI data observations.

Two inner Linblad resonances, located at 0.4 and 2.5 kpc, and an outer Linblad resonance at $R = 18 \text{ kpc}$, are obtained for a pattern speed of $\Omega_p = 20 \text{ km s}^{-1} \text{kpc}^{-1}$.

The determination of the *ILR* radii is crucial for understanding the complex structure observed in H α and CO in the centre of NGC 4321. In Sect. 2 we have described its morphology and now, we will thoroughly compare it, with the best fit of the simulations.

Figure 10 shows the morphology in the inner 3 kpc radius, from H α (Knapen 1992) (a) and interferometric CO observations (Canzian 1989) (b). Figure 10c displays the particle orbits from partially inelastic collisions for an $\Omega_p = 20 \text{ km s}^{-1} \text{kpc}^{-1}$ in the same region. In the three cases we can see a displacement of the rotation centre respect to the optical one. There are three concentrations of CO and H α emission, following the main bar axis and located diagonally to the rotation centre at $\sim 0.5 \text{ kpc}$ radius. Another two weaker concentrations of emission can be seen above and below of the centre at a distance of $\sim 0.3 \text{ kpc}$ radius. We could interprete this emission enhancement in both the CO and H α maps as the signature of the *ILR*'s. In fact, we can clearly see in Fig. 11c the crossing of orbits corresponding to the regions delimited by the *ILR*'s at $\sim 0.5 \text{ kpc}$ (ILR_1) and $\sim 2.5 \text{ kpc}$ (ILR_2). A higher molecular gas collision rate, could increase the formation of GMC's and subsequently the star for-

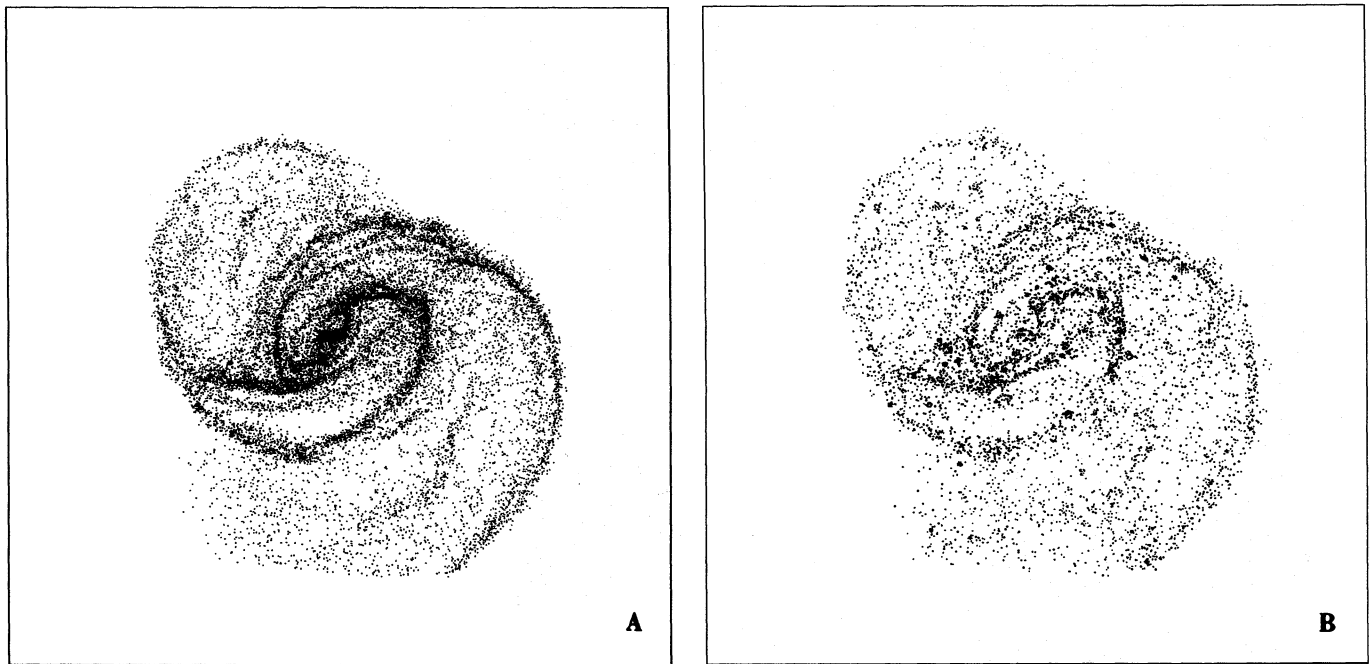


Fig. 13a and b. Particle plots of the molecular clouds distribution in the NGC 4321 disc for the best fit $\Omega_p = 20 \text{ km s}^{-1} \text{ kpc}^{-1}$. **a** Partially inelastic collisions. **b** Inelastic collisions

mation. The same effect could explain the strong H α emission at the edges of the main bar.

Figure 11 shows the intensity contours of the molecular gas overlaid on the potential in the inner 5 kpc radius. The misalignment between the small oval potential and the molecular gas is evident as expected from dynamical behaviour of the gas near the ILR's: there exist perpendicular periodic orbits (x_2) in the centre. The gas clouds tend to follow these orbits but due to collisions, they only gradually turn from a parallel to perpendicular alignment to the bar. In this way, the gas response advances with respect to the gravitational potential.

We have discussed in Sect. 3 the intrinsic uncertainties on the application of the Canzian test for a “real” galaxy. We can evaluate critically the importance of these limitations by applying the test to the four different outputs of the simulations. In the simulations we have a priori knowledge of both the rotation curve and the dynamic centre, so undesirable factors are completely eliminated. Figure 12 shows the results of the Canzian test applied to the two extreme values of the simulation runs. The best fit, $\Omega_p = 20 \text{ km s}^{-1} \text{ kpc}^{-1}$, has already been discussed in Sect. 4 (see Fig. 3d).

In all cases the approaching and receding sides have the same disc area and they show a beautiful global symmetry. The transition from the $m=3$ mode to the $m=1$ mode can be clearly assessed for $\Omega_p = 25$. For $\Omega_p = 10$ the corotation ellipse is located at the boundaries of the disc and the $m=1$ barred mode occupies the entire disc area.

In the previous Subsect. 5.2 we presented several runs of simulations with different models that we have carried out to

test the influency of the dissipation and the self-gravity in our fit.

As advanced in Paper I, the final configurations from the first and second models (inelastic and partially inelastic collisions) are very similar (see Fig. 13), revealing that the amount of dissipation after a complete run is not a decisive factor in the dynamical evolution of the whole gas disc. Nevertheless, in the centre of the galaxy the collision rate is higher due to the crossing orbits caused by both ILR's, and dissipation effects are more evident.

In the third model (self-gravitating), the behaviour of the gas is locally different, more clumpy, and the spiral arms are thinner and more contrasted, but the relative position of the gaseous arms is the same as in the non self-gravitating case (see Fig. 14). This is far to be surprising: the total amount of gas in this galaxy ($\sim 7\%$) is kept low enough not to be an important contributor to the gravitational potential.

From these results we can reassure the validity of our fit and confirm that all the features of the tracers (gas plus red image) used in this paper seem to be in good agreement with the results of the best fit of the simulations.

5.5. The line-widths maps

In this section we analyse the velocity dispersion maps for the 30m CO data, the simulations and the HI data cube. Our intention is to study the influence of the density wave on the measured velocity dispersion, in particular its variation depending on the location on the disc (arm, interarm and centre regions).

The 30m map is limited to a strip covering the minor axis region, so we have no complete 2-D picture of the behaviour of

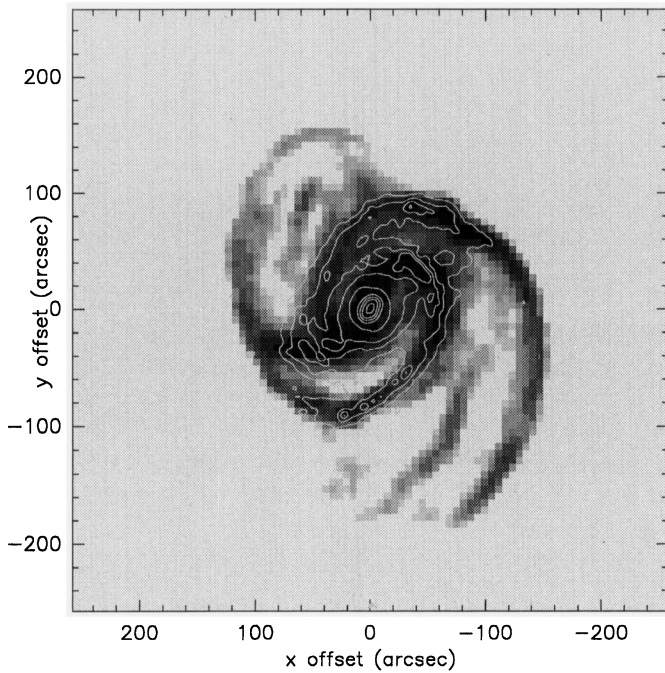


Fig. 14. Superposition of the simulated response of the gas disc in the self-gravitating model (grey scale) and the red image (solid contours) for $\Omega_p=20 \text{ km s}^{-1} \text{ kpc}^{-1}$, the best fit

velocity dispersion for the molecular gas. Nevertheless, a slight enhancement of the velocity dispersion is visible in the 30m CO spectra taken along the minor axis strip when we approach the spiral arms (See Fig. 4). This is especially true for the SE arm spectra when they are compared with the spectra of the adjacent interarm region. The on-arm average spectrum has a linewidth of 35 km s^{-1} , a factor of 1.2 higher than the average interarm spectrum.

Although it could be argued that the regions concerned are located at different galactocentric distances (so being affected by different rotation velocity gradients) we believe that this effect might be attributed to a different cloud-cloud velocity dispersion or eventually to molecular cloud populations being different in the arm and in the interarm regions. However, the differences in velocity dispersion between arm and interarm regions are much more important in M 51 than in NGC 4321. Garcia-Burillo et al. (1993), found evidences of macroscopic opacity effects, i.e., molecular clouds surface filling factor being close to one, in M 51. This, together with spatially unresolved streaming motions (particularly large in M 51), might partly explain why linewidths are so large in some on-arm regions of this galaxy.

On the other hand, CO emission seems to be much more centrally peaked in NGC 4321: for the region where the two average spectra have been taken in the disc of NGC 4321, the derived gas column density is a factor of 4 smaller than the one derived for a typical arm-region in M 51. So we expect no significant contribution of macroscopic opacity effects to the observed CO line widths in spiral arms for NGC 4321. It should

also be noted that the inclination angle for M 51 is smaller than for NGC 4321 ($i(\text{M 51})=20$, $i(\text{NGC 4321})=32$): Given a total gas column density, the surface filling factor in each channel diminishes when the inclination of the galaxy is higher. What is even more important: streaming motions are also expected to be of a lesser order of magnitude in NGC 4321 than in M 51 (NGC 5194 has a strong density wave probably induced by the passage of the companion NGC 5195). Consequently, the widening effect of unresolved streaming motions within our lobe would be less important in M100 than in M 51.

We have computed the velocity dispersion maps for the best fit simulation cube, $\Omega_p=20 \text{ km s}^{-1} \text{ kpc}^{-1}$ and for the 20''HI data cube (see Fig 15). The gradient of the rotation curve within the beams has not been subtracted.

Although we are limited by the scarce velocity resolution of the HI data ($\Delta v=21 \text{ km s}^{-1}$), there is a noticeable enhancement of the velocity dispersion along the spiral arms and the gaseous molecular bar in both the simulations and the observations.

We show in Fig. 16 two spectra typical of an interarm and arm region, obtained by averaging the emission on two regions of similar spatial extent and located and including a comparable contribution from galactic rotation gradient to the observed linewidths. The difference in the linewidths must necessarily come from a mixture of different cloud-cloud velocity dispersions or different residual large-scale velocity gradients coming from streaming motions. Note that in the simulations the difference in the internal cloud velocity dispersion along the arms or the interarm regions plays no role in the final result (clouds follow the same size-linewidth relationship everywhere in the disc).

The widening of the on-arm HI spectra seems to hold for the whole disc of NGC 4321 (by a factor of 1.5 approximately). Though the on-arm spectrum of the simulations shown has a non gaussian shape, we estimate the widening factor of the spectra to be similar both in the simulated gas spectrum and in the observations.

Probably the same explanation accounts for the difference in linewidths between the arm and the interarm region for HI and CO (both the “simulated” and the “observed” map).

Our results are in contradiction with other models which get lower dispersion in the arms than the interarms (see Rydbeck et al. 1991; Thomasson et al. 1991). This is probably due to the fact that in these models the formation of GMC's and the star formation are not included. The cloud coagulation is not compensated by the injection of energy after star formation and consequently the dispersion of the conglomerates, that follows the \sqrt{N} law, is lower in the arms where there is a greater collision rate of particles.

6. Conclusions

Reliable estimates of pattern speeds (Ω_p) in the discs of spiral galaxies are difficult to obtain: Ω_p is not a directly observable parameter and therefore the different methods applied so far rely on theoretical assumptions or they are model dependent. Therefore, it is hardly surprising that the practical application

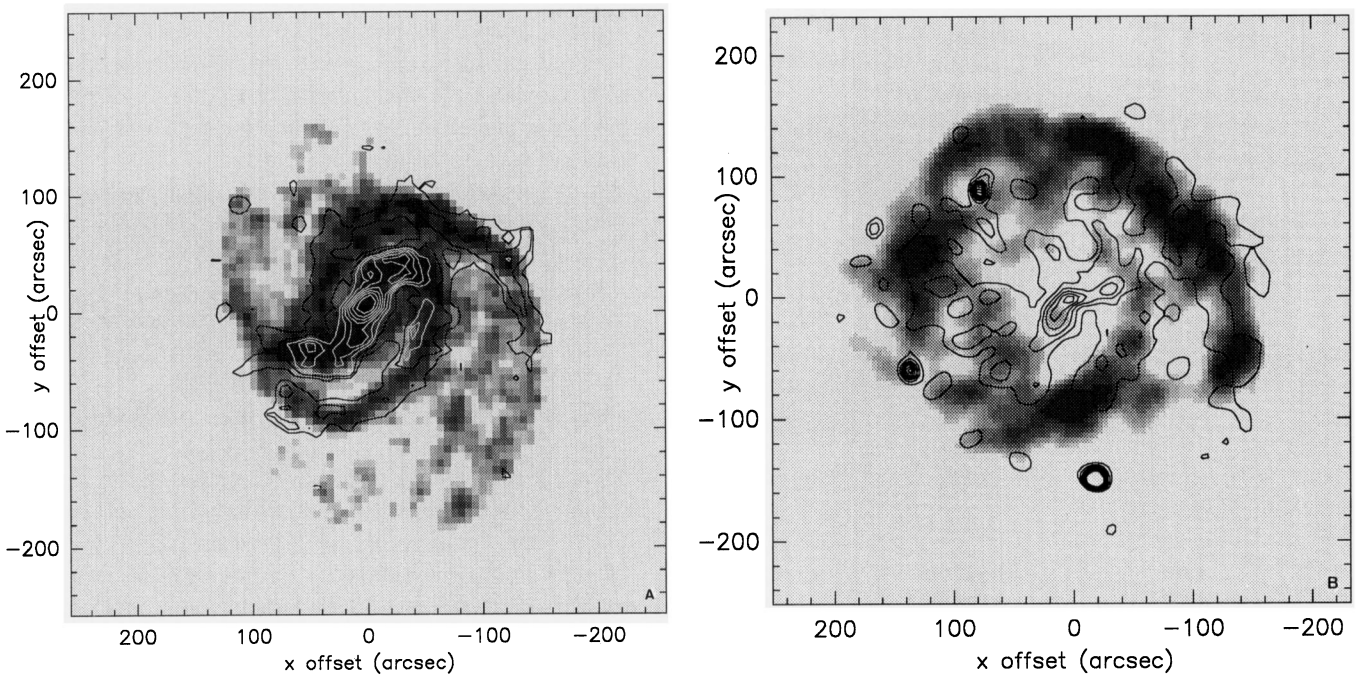


Fig. 15a and b. Contours of velocity dispersion (from 10 to 50 by 5 km/s) superposed on **a** the simulations intensity map, **b** the HI observations. An enhancement of velocity dispersion along the stellar bar and the spiral arms stands out clearly

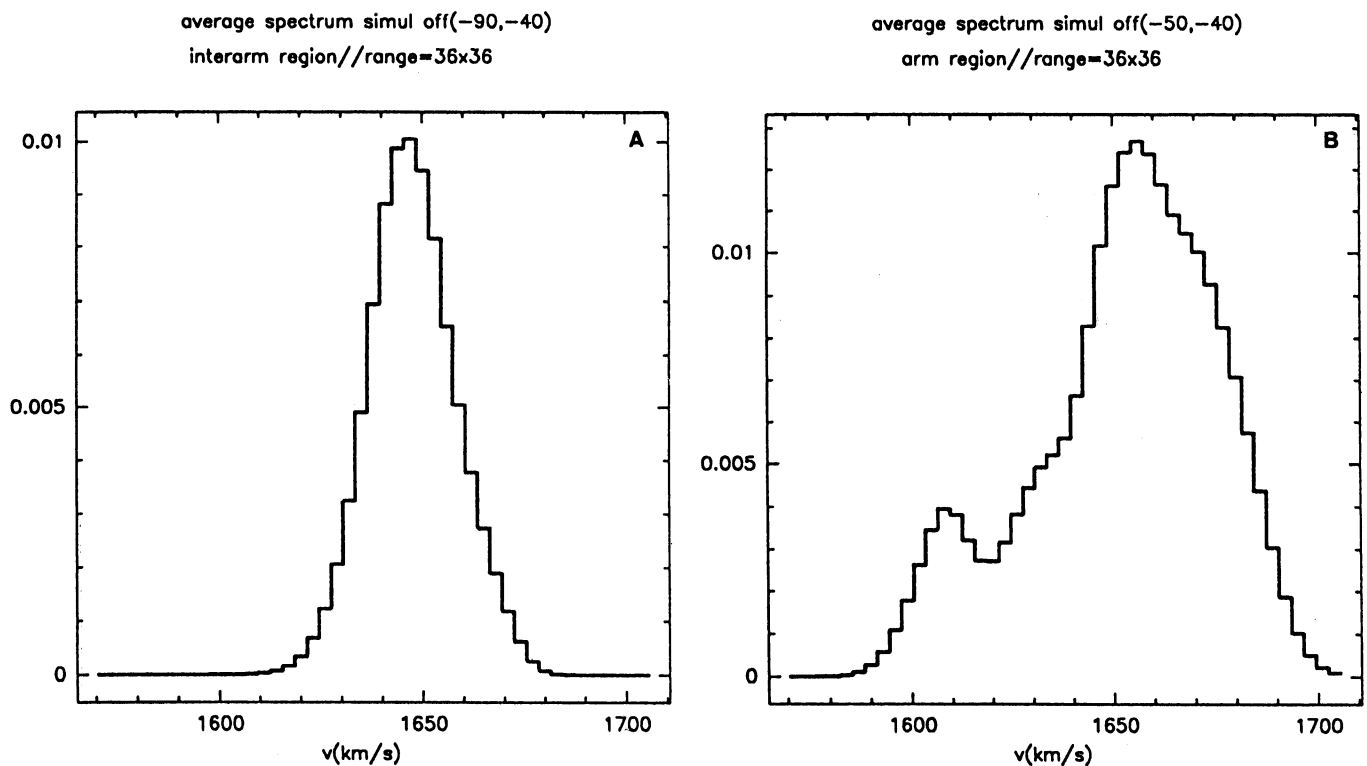


Fig. 16a and b. The CO (simulations) emission spectra taken at two typical interarm and arm regions of NGC 4321 centred at (x,y) offsets (-90,-40) and (-50,-40) respectively. The emission has been averaged on squared regions of extension $34'' \times 34''$, in order to get a higher signal to noise ratio

of these methods for real galaxies give different if not clearly contradictory results.

In this paper we discuss the validity of two different and completely independent methods to determine pattern speeds in the discs of spiral galaxies and applied them to the grand design spiral NGC 4321.

Our choice seems justified because NGC 4321 possesses a well defined mode in its disc (and so a predominant value of Ω_p) since the galaxy is barred.

The first method, discussed by Canzian (1993), is based on the expected sign reversal of the radial streaming motions when we go across the corotation resonance. Although it relies on the validity of a theoretical prediction, its application to real galaxies is entirely based on observations. As we consider the global disc gas response to derive the position of the corotation resonance, contrary to other observations-based tests, this method should be reasonably accurate.

The second method consists of a model fitting of the observed gas plus stellar spiral structure, performed with numerical simulations of the cloud hydrodynamics. This method furnishes an estimate of the pattern speed of the spiral wave (the free parameter of the model) to be compared with the one provided by the Canzian test.

In a previous work (Paper I), we applied the method of the reversal of the radial streaming motions to the minor axis of the galaxy and compared the results with a set of preliminary numerical simulations. Both methods gave completely different solutions. As already explained, we attributed the apparent absence of the signature of corotation in the CO minor axis position-velocity diagram to the absence of a well defined transition between the oval orbits (typical of the region inside corotation) and the figure eight orbits (outside corotation). The results derived from the Canzian test help to clarify the reasons behind such contradiction. Due to the morphology of this galaxy, strongly distorted by the bar, the minor axis crosses over a region where "there is not" a reversal of the radial streaming motions after corotation. The minor axis happens to coincide with an outer prolongation of the inner mode pair (I1a, I1r) obtained in the Canzian test, more precisely, with the trailing outer pair (O2a, O2r). As we advanced in Paper I making strips along other directions in the disc we can find a sign reversal of the radial streaming motions.

Deriving a precise value of Ω_p requires a global view of the gas kinematics in the whole galaxy disc. Both the Canzian test and the numerical simulations use the maximum amount of information from observations.

We summarize the main results of this work as follows:

- We have taken the HI velocity field derived from the 20''VLA map of Knapen et al. (1993) to apply the Canzian test in NGC 4321. Although HI is deficient within the inner 9 kpc, its emission covers the entire optical disc. We have used the model of Shu et al. (1973) to study in detail the expected morphology of the residual velocity field in a barred spiral galaxy depending on the wave pattern speed (Ω_p). We can clearly identify in the HI velocity map one pair of approaching-receding spiral arms from the centre up to

the disc edge. Two additional pairs of approaching-receding arms stretch out symmetrically from a distance of $R \sim 11$ kpc. This is exactly the expected theoretical pattern if corotation is located at this distance, lying in the middle of the disc. The transition zone between the m=1 mode and the m=3 mode extent from 8 kpc to 11 kpc.

- The second method described in this paper, based on numerical simulations, furnishes a value of Ω_p in excellent agreement with the one provided by the Canzian test (the best fit solution corresponds to $\Omega_p = 20 \text{ km s}^{-1} \text{ kpc}^{-1}$, i.e. $R_{CR} \sim 11 \text{ kpc}$). The gas response is very sensitive to the trial value of Ω_p , therefore R_{CR} as well as the position of the remaining principal resonances in the disc (two ILR's at 0.4 and 2.5 kpc respectively and an OLR at 18 kpc) are accurately determined.
- The estimated position of the ILR's offers a satisfactory explanation for the observed peculiar morphology of the NGC 4321 centre. At close sight, the particle orbits diagram in the simulations shows that the gas clouds in the region located between the two ILR's tend to follow the x_2 orbits (perpendicular to the main bar potential). The transition towards the x_1 orbits domain takes place at the outer ILR (x_1 orbits dominates between the outer ILR and corotation). We interpret the enhancement of the emission visible in the H α and CO interferometric maps as a direct consequence of the orbit crossing at the inner ILR that may increase the cloud-cloud collision rate and therefore favour the formation of GMC's and subsequently the star formation activity.
- Finally, we have studied the line-widths in the HI, CO and simulations maps and concluded that velocity dispersion is higher in the arms and close to the centre than in the interarm region. We interpret this difference in terms of a lower cloud-cloud and internal velocity dispersions characteristic of the interarm regions.

From the derived value of the pattern speed in NGC 4321, we can assert that corotation is in the middle of the disc. The stellar bar ends before corotation, and the spiral arms reach the OLR located at the optical disc edge.

The Canzian test reveals as a optimum method to detect the presence of density waves in the discs of spiral galaxies and to derive their pattern speeds with reasonable accuracy. We insist on the relevance of an accurate determination of pattern speeds in understanding the origin and mechanism of maintenance of spiral density waves.

Acknowledgements. The numerical simulations presented in this paper have been done using the VP-200 of the "Centre de Calcul Vectoriel pour la Recherche" (CCVR), Ecole Polytechnique, Palaiseau (France). We are grateful to B.Elmegreen for his useful comments and discussions. M.J.Sempere thanks the CNRS (France) and the IAC (Spain) for their economic support during this work. S.García-Burillo thanks the Spanish CICYT for its partial economic support (grant number PB90-408).

References

- Arsenault, R., Boulesteix, J., Georgelin, Y., Roy, J-R., 1988, A&A, **200**, 29
- Arsenault, R., Roy, J.R., Boulesteix, J., 1990, A&A, **234**, 23
- Canzian, B., 1989, in "The interstellar medium in external galaxies", Wyoming, NASA conference publication 3084
- Canzian, B., 1992, *Ph.D., CALTECH, Astronomy Department, USA*
- Canzian, B., 1993, ApJ, **414**, 487
- Casoli, F., Combes, F., 1982, A&A, **110**, 287
- Cayatte, V., van Gorkom, J.H., Balkowski,C., Kotanyi,C., 1990, ApJ, **100**, 604
- Cepa, J., Beckman, J.E., 1990, AJ, **349**, 497
- Cepa, J., Beckman, J.E., 1990, A&AS, **83**, 211
- Cepa, J., Beckman, J.E., Knapen, J.H., Nakai, N., Kuno, N., 1992, AJ, **103**, 429
- Combes, F., Gerin, M., 1985, A&A, **150**, 327
- Combes, F., Debbash, F., Friedli, D., Pfenniger, D., 1990, A&A, **233**, 82
- Combes, F., Elmegreen, B.G., 1993, A&A, **271**, 391
- Combes, F. in "Mass-Transfer Induced Activity in Galaxies", 1994, Lexington, Proceedings, I. Shlosman (eds), p.
- Elmegreen, B.G., Elmegreen, D.M., Seiden, Ph.E., 1989, ApJ, **343**, 602
- Friedli, D., Martinet, L., 1993, A&A, **277**, 27
- García-Burillo, S., Sempere, M.J., Combes, F., 1994, A&A (in press)
- García-Burillo, S., Combes, F., Gerin, M., 1993, A&A **274**, 148
- Guhathakurta, P., van Gorkom, J.H., Kotanyi, C.G., Balkowski, C., 1988, AJ, **96**, 851
- Kenney, J.D., Young, J.S., 1988, ApJS, **66**, 261
- Kent, S.M., 1987, AJ, **63**, 1062
- Kent, S.M., Glaudell, G., 1989, AJ, **98**, 1588
- Knapen, J.H., 1992, Ph.D., Universidad de La Laguna, SPAIN
- Knapen, J.H., Beckman, J.E., Cepa, J., van der Hulst, J.M., Rand, R.J., 1992, ApJ, **385**, L37
- Knapen, J.H., Cepa, J., Beckman, J.E., del Rio, M.S., Pedlar, A., 1993, ApJ, **416**, 563
- Pierce, M.J., 1986, AJ, **92**, 285
- Rubin, V.C., Ford, W.K., Thonnard, N., 1980, AJ, **238**, 471
- Rydbeck, G., Bergman, P., Hjalmarson, Å., Thomasson, M., Wiklind, T., 1991, in "Dynamics of Disc Galaxies", Göteborg Proceedings, B. Sundelius (eds.), p. 235-239
- Sandage, A., Tamman, G. A., 1987, *A revised Shapley-Ames Catalog of Bright Galaxies*, Second Edition, Carnegie Institution of Washington publication 635, Washington D.C.
- Shu, F., 1973, ApJ, **183**, 819
- Thomasson, M., Donner K.G., Elmegreen, B., 1991, in "Dynamics of Disc Galaxies", Göteborg Proceedings, B. Sundelius (eds.), p. 279-283
- Tremaine, S., Weinberg, M.D., 1985, ApJ, **282**, L5
- Van der Bergh, S., 1989, A&AR, **1**, 111
- Vaucoleurs, G. de, Vaucoleurs, A. de, Corwin, H.G., Buta, R.J., Paturel, G., Fouqué, P., 1991, *Third Reference Catalogue of Bright Galaxies*, Springer Verlag, New York.
- Young, J.S., Scoville, N.Z., Brady, E., 1985, ApJ, **288**, 487
- Young, J.S., Scoville, N.Z., 1991, ARA&A, **29**, 581
- Warmels, R.H., 1988, A&A, **72**, 19